Ketogenesis acts as an endogenous protective programme to restrain inflammatory macrophage activation during acute pancreatitis

Li Zhang,[a] Juanjuan Shi,[a] Dan Du,[b,c] Ningning Niu,[a] Shiyu Liu,[b] Xiaotong Yang,[a] Ping Lu,[a] Xuqing Shen,[a] Na Shi,[b] Linbo Yao,[b] Ruling Zhang,[d] Guoyong Hu,[d] Guotao Lu,[e] Qingtian Zhu,[e] Tao Zeng,[f] Tingting Liu,[b] Qing Xia,[b] Wei Huang,[b,g]* and Jing Xue[a]*

[a]State Key Laboratory of Oncogenes and Related Genes, Stem Cell Research Centre, Shanghai Cancer Institute, Ren Ji Hospital, Shanghai Jiao Tong University School of Medicine, 160 Pujian Rd, Shanghai 200127 China
[b]Department and Laboratory of Integrated Traditional Chinese and Western Medicine, Sichuan Provincial Pancreatitis Centre and West China-Liverpool Biomedical Research Centre, West China Hospital, Sichuan University, 37 Guoxue Alley, Chengdu 610041, China
[c]Advanced Mass Spectrometry Centre, Research Core Facility, Frontiers Science Centre for Disease-related Molecular Network, West China Hospital, Sichuan University, Chengdu 610041, China
[d]Shanghai Key Laboratory of Pancreatic Disease, Institute of Pancreatic Disease, Shanghai Jiao Tong University School of Medicine, Shanghai 200127, China
[e]Department of Gastroenterology, Pancreatic Centre, Affiliated Hospital of Yangzhou University, Yangzhou University, Yangzhou 225001, China
[f]Zhangjiang Laboratory, Institute of Brain-Intelligence Technology, Shanghai, China
[g]Institutes for Systems Genetics & Immunology and Inflammation, Frontiers Science Centre for Disease-Related Molecular Network, West China Hospital, Sichuan University, Chengdu 610041, China

eBioMedicine 2022;78: 103959
Published online 25 March 2022
https://doi.org/10.1016/j.ebiom.2022.103959

Summary

Background Innate immunity and metabolites link to the pathogenesis and severity of acute pancreatitis (AP). However, liver metabolism and its role in immune response and AP progression remain elusive. We investigated the function of liver metabolism in the pathogenesis of AP.

Methods Circulating ketone body β-hydroxybutyrate (βOHB) levels were determined in AP clinical cohorts and caerulein-induced AP (CER-AP) mouse models receiving seven (Cer*7) or twelve (Cer*12) injection regimens at hourly intervals. Liver transcriptomics and metabolomics were compared between CER-AP (Cer*7) and CER-AP (Cer*12). Inhibition of fatty acid β-oxidation (FAO)-ketogenesis, or supplementation of βOHB was performed in mouse models of AP. The effect and mechanism of βOHB were examined *in vitro*.

Findings Elevated circulating βOHB was observed in patients with non-severe AP (SAP) but not SAP. These findings were replicated in CER-AP (Cer*7) and CER-AP (Cer*12), which manifested as limited and hyperactive immune responses, respectively. FAO-ketogenesis was activated in CER-AP (Cer*7), while impaired long-chain FAO and mitochondrial function were observed in the liver of CER-AP (Cer*12). Blockage of FAO-ketogenesis (Cpt1a antagonism or *Hmgcs2* knockdown) worsened, while supplementation of βOHB or its precursor 1,3-butanediol alleviated the severity of CER-AP. Mechanistically, βOHB had a discernible effect on pancreatic acinar cell damage, instead, it greatly attenuated the activation of pancreatic and systemic proinflammatory macrophages via class I histone deacetylases.

Interpretation Our findings reveal that hepatic ketogenesis is activated as an endogenous protective programme to restrain AP progression, indicating its potential therapeutic value.

*Corresponding author at: State Key Laboratory of Oncogenes and Related Genes, Stem Cell Research Centre, Shanghai Cancer Institute, Ren Ji Hospital, Shanghai Jiao Tong University School of Medicine, 160 Pujian Rd,Shanghai, 200127, China.
*Corresponding author: Department and Laboratory of Integrated Traditional Chinese and Western Medicine, Sichuan Provincial Pancreatitis Centre and West China-Liverpool Biomedical Research Centre, West China Hospital, Sichuan University, 37 Guoxue Alley, Chengdu, 610041, China.
E-mail addresses: dr_wei_huang@scu.edu.cn (W. Huang), jingxue@sjtu.edu.cn (J. Xue).

Funding This work was supported by the National Natural Science Foundation of China, Shanghai Youth Talent Support Programme, and Shanghai Municipal Education Commission-Gaofeng Clinical Medicine Grant.

Keywords: Acute pancreatitis; Fatty acid β-oxidation; β-Hydroxybutyrate; Macrophage; Class I HDACs

Research in context

Evidence before this study

AP is an inflammatory disease with increasing global incidence and no active therapy. Innate immunity and metabolites link to the pathogenesis and severity of AP, but little is known about how liver metabolism affects AP progression.

Added value of this study

Hepatic FAO-ketogenesis is activated in mild AP but not in its more severe form. Defective long-chain FAO and mitochondrial dysfunction result in insufficient ketogenesis. Endogenous and dietary βOHB improves the severity of AP by limiting proinflammatory macrophage activation.

Implications of all the available evidence

Strategies to activate endogenous ketogenesis or direct supplementation with exogenous βOHB may be promising for the prevention and treatment of AP.

Introduction

Acute pancreatitis (AP), like most acute inflammatory responses, when mild is a self-limiting disease that can resolve with minimal treatment.[1] However, patients with severe AP (SAP) characterised as developing persistent or multiple organ failure can have a mortality rate of > 30%.[2–4] Currently, no active therapy exists for AP due to limited understanding of its pathogenesis.[1] Accumulating evidence suggests that inflammatory monocytes and macrophages determine the severity of this disease.[5] Therefore, targeting these immune cells might be a therapeutic strategy against AP.[5–7] Liver metabolism and the innate immune response are finely orchestrated processes in various physiological and pathophysiological conditions.[8,9] Liver injury is common albeit overlooked in both experimental and human AP where Kupffer cells may act as the amplifier that translates pancreatic injury into a systemic inflammatory cascade.[10] Despite some endogenous metabolites are released during AP,[11] how liver metabolites and metabolic processes affect pancreatic and systemic inflammatory responses and vice versa remains elusive.

During AP, the inappropriate pancreatic lipase release not only initiates autodigestion of the pancreas, but also induces excessive lipolysis of pancreatic and visceral adipose tissues.[12–14] This process, if uncontrolled, generates an overwhelmed amount of nonesterified fatty acids (NEFAs), which in turn aggravate the damage to pancreatic acinar cells and even lead to organ failure.[12,13,15] The liver serves as a metabolic hub responsible for maintaining the homeostasis of fatty acids, glucose, and amino acids.[16] Fatty acid β-oxidation (FAO) is a major catabolic process that degrades long-chain (LC) acyl-CoA to acetyl-CoA,[17] which then enters the tricarboxylic acid (TCA) cycle or ketogenesis process for energy production. In response to fasting or stress, hepatic ketogenesis turns FAO-derived acetyl-CoA into ketone bodies such as acetoacetate (AcAc) and β-hydroxybutyrate (βOHB) to serve as alternative energy fuels for extrahepatic tissues.[16] Of note, the role of ketone bodies as signalling mediators to modulate critical cellular events has been increasingly recognised recently.[16] For example, βOHB itself could act as a histone covalent modifier at lysine residues in hepatocytes[18] and $CD8^+$ T cells.[19] βOHB mainly functions as a ligand for G protein-coupled receptors GPR109A/HCAR2 and GPR41/FFAR3, which are involved in liver injury, neurodegenerative diseases, and sympathetic depression.[20–22] Moreover, βOHB has been shown to block lipopolysaccharide (LPS)-induced inflammation by suppressing the canonical NLRP3 inflammasome in murine bone marrow-derived macrophages (BMDMs).[23] In addition, it also attenuates oxidative stress via inhibition of class I histone deacetylases (HDACs) in HEK293 cells,[24] but whether the same mechanism applies in BMDMs awaits assessment.

In this study, we found that circulating ketone body βOHB was elevated in both human and experimental AP. By using comprehensive analyses of the transcriptome and targeted metabolome of livers from experimental AP mice, we identified carnitine palmitoyl transferase 1-alpha (CPT1α)- and hepatic 3-hydroxy-3-methylglutaryl-CoA synthase 2 (HMGCS2)-mediated FAO-ketogenesis process as a key mechanistic link between the inflamed pancreas and liver metabolism. However, the insufficient ketogenesis in more severe

AP compared with its mild form in mice was largely attributed to impaired LC-FAO and mitochondrial dysfunction of hepatocytes. Exogenous supplementation of ketone bodies (βOHB or its precursor) greatly ameliorated pancreatic and systemic injuries by restraining the activation of proinflammatory macrophages. Herein, these findings highlight the hepatic ketogenesis as an endogenous protective programme in control of the inflammatory response during AP progression and imply its therapeutic potential.

Methods

Human samples

Two independent cohorts were used in our study. AP was diagnosed according to the revised Atlanta classification.[25] Cohort 1: Partial plasma samples were from a previously described cohort[26] comprising healthy volunteers and AP patients (n = 41) admitted to Shanghai General Hospital. Cohort 2: Clinical data were obtained as previously described[27] from surviving AP patients (n = 211) in the West China Biobanks of Sichuan University between December 2017 and June 2019. Patients were further excluded if comorbid diabetes and severe liver diseases existed. Patients in both cohorts were admitted within 48 h after abdominal pain onset and blood was withdrawn as soon as possible.

Mice

BALB/c mice (6-8 weeks old) were purchased from Shanghai SLAC Laboratory Animal Co. Ltd (Shanghai, China). *Hca2*$^{-/-}$ mice were obtained from Dr Stefan Offermanns (Max-Planck-Institute Bad Nauheim) and generated as described previously.[28] *Ffar3*$^{-/-}$mice were purchased from the Model Animal Research Centre of Nanjing University (Nanjing, Jiangsu Province, China). All genetically modified mice and their wild type (WT) littermates were on a C57BL/6J background. All mice were housed under conditions of controlled temperature (22−25°C) and humidity (40−60%) with a 12:12 h light-dark cycle and were allowed free access to water and food.

Ethics

Patient-informed consent was obtained according to the study protocol, which was approved by the ethics committee of Shanghai General Hospital (Cohort 1: Approval No. RA-2019-213) and West China Hospital of Sichuan University (Cohort 2: Approval No. 2017[456]). All animal husbandry and procedures were approved by the Animal Care and Use Committee at Renji Hospital (RJ2020-0505), Shanghai Jiao Tong University School of Medicine.

Mouse models and treatments

Age- and sex-matched Balb/c mice were used in the following experiments. To avoid the effect of prefasting on the synthesis of ketone bodies in mice, we fasted mice only during the injection process and food was provided immediately after the last injection. Mouse models included (1) hourly intraperitoneal injections of 50 or 100 μg/kg caerulein (Yeasen Biotech) dissolved in normal saline for 7 times to induce necrotising AP (CER-AP [Cer*7]) without marked systemic inflammation[29]; (2) hourly intraperitoneal injections of 100 μg/kg caerulein 12 times to induce more severe necrotising AP (CER-AP [Cer*12]) with overt lung and liver injuries[29,30]; (3) and LPS (10 mg/kg; Sigma Aldrich) superimposed on a Cer*7 regimen right after the last injection of caerulein to induce necrotising SAP (CER/LPS-SAP) mimicking septic conditions with multiple organ failure.[31] Control mice received saline injections following the respective regimens. All animals were sacrificed at 24 h after first caerulein or saline injection unless otherwise mentioned.

For treatments, the Balb/c mice were (1) fed with 1,3-butanediol (5.72% (w/v); Sigma-Aldrich) or normal water (control) one week before disease induction; (2) received a single intraperitoneal injection of βOHB (3 mmol/kg; Sigma-Aldrich) or normal saline at the indicated time; and (3) the CPT1α inhibitor etomoxir (20 mg/kg, Sigma-Aldrich), histone deacetylase (HDAC) pan inhibitor TSA (0.1 mg/kg; Targetmol), HDAC1/3 inhibitor MS-275 (20 mg/kg; Targetmol), or dimethyl sulfoxide (DMSO) as a control 1 h before disease induction.

For *in vivo* gene silencing of hepatic *Hmgcs2*, Balb/c mice were injected with sh-Con (negative control) or sh-Hmgcs2 wrapped with lentivirus via tail vein injection (1×10^8 TU per mouse). Three weeks later, these mice were subjected to the Cer*7 regimen. Liver *Hmgcs2* mRNA and serum βOHB levels were measured to assess knockdown efficiency. The shRNA sequence was shHmgcs2 5′-CCATGTCTGTCTACACGAA-3′.

Cell isolation and culture conditions

Pancreatic leukocytes were isolated using the collagenase digestion method described for flow cytometry analysis.[32] Liver cells and spleen cells were acquired by simply smashing tissues and then washing with FACS buffer (HBSS + 2% NCS) for subsequent staining. Pancreatic acinar cells were isolated using collagenase I (0.2 mg/ml; Yeasen Biotech) and IV (0.2 mg/ml; Yeasen Biotech), shaken at 37°C for 10 min, and then dissociated with tips. Acinar cells were stimulated with caerulein (1×10^{-7} M) for 5 h before conditioned medium collection. Bone marrow cells were cultured with recombinant mouse M-CSF (50 ng/ml; Novoprotein, Suzhou, China) to generate BMDMs as previously described.[33] On day 6 of culturing, BMDMs were

stimulated with LPS (100 ng/ml) for 15 min or 4 h, or injured acinar cell culture medium for further assays. βOHB (10 mM; Sigma-Aldrich), HDAC pan-inhibitor TSA (1 μM; MedChem Express, Shanghai, China) or HDAC1/3 inhibitor MS-275 (20 μM; MedChem Express) was administered 1 h before LPS stimulation.

RNA-seq and analysis

For liver RNA preparation, liver tissues from 6-week Balb/c mice of designated groups were harvested at 24 h. For BMDM RNA preparation, 1×10^6 cells were pretreated with phosphate-buffered saline (PBS) or βOHB for 1 h before LPS administration and then harvested at 4 h thereafter.

The RNA-seq transcriptome library was prepared following the TruSeqTM RNA Sample Preparation Kit (Illumina) using 5 μg of total RNA, according to the manufacturer's instructions. The raw paired end reads were trimmed and quality controlled, and then clean reads were separately aligned to the reference genome with orientation mode using TopHat (version 2.0.0). To identify differentially expressed genes (DEGs) between two different groups, the expression level of each transcript was calculated according to the FPKM. RSEM was used to quantify gene abundances. The R statistical package software EdgeR (Empirical analysis of Digital Gene Expression in R) was utilised for DEG analysis. In addition, functional-enrichment analyses including GO and KEGG were performed to identify which DEGs were significantly enriched in GO terms and metabolic pathways at a Bonferroni corrected p value ≤ 0.05 compared with the whole transcriptome background. Gene Set Enrichment Analysis (GSEA; http:/www.broadinstitute.org/gsea/index.jsp) of the expression data was used to assess enrichment of the KEGG and GO gene sets.

Targeted metabolome profiling and analysis

Liver tissues from the designated groups harvested at 24 h were perfused with cold 5 ml PBS, and then rapidly removed into liquid nitrogen for storage. Samples (approx. 10 mg for each) were homogenised with methanol to extract the metabolites, followed by mixing with internal standards. Subsequently, the derivatized samples were subjected to ultra-performance liquid chromatography coupled to a tandem mass spectrometry (UPLC-MS/MS) system (ACQUITY UPLC-Xevo TQ-S, Waters Corp.) to quantitate the metabolites. All standards were obtained from Sigma-Aldrich. The quality control samples were prepared following the same procedures as the test samples and were injected every 14 test samples to ensure reproducibility. Raw data from UPLC-MS/MS analysis were analysed using MassLynx software (v 4.1, Waters Corp.) to calculate the concentration of each analyte in the samples. Univariate and multivariate analyses were both performed in R studio (http://cran.r-project.org/). In addition, enrichment analysis was performed with MetaboAnalyst 4.0 (www.metaboanalyst.ca), a comprehensive server for metabolomic data analysis based on KEGG metabolic pathways. Targeted metabolome profiling of mouse livers was performed by Metabo-Profile (Shanghai, China).

Histology

The pancreas and other tissues were fixed in 10% formalin overnight, and then were sectioned and stained with haematoxylin-eosin (prepared by Servicebio Inc, Wuhan, China). The severity of AP was scored in a blinded way as described previously.[34,35]

Briefly, histopathology scores ranging from 0 to 9, including pancreatic oedema, inflammation, and necrosis, were used to indicate the pancreatic injury. Oedema was scored from 0 to 3 (0: absent; 1: locally enlarged between the lobules; 2: diffusely enlarged between lobules; 3: acini ruptured and separated), inflammation was scored from 0 to 3 (0: absent; 1: few immune cells in pancreatic margins; 2: few immune cells scattered between lobule; 3: vast immune cells scattered between lobule), and acinar necrosis was scored from 0 to 3 (0: absent; 1: pancreatic periductal necrosis; 2: locally necrosis; 3: diffusely necrosis).

βOHB assessment

Plasma or serum from humans or mice was diluted in PBS, and βOHB levels were determined by a Fluorometric Assay Kit (Cayman, MI, USA) according to the manufacturer's instructions. Fluorescence intensity was measured by a fluorescence microplate reader (GloMax® Discover Microplate Reader, Promega).

Liver mitochondria isolation and analyses

For the isolation of liver mitochondria, fresh liver tissues were cut into small pieces to isolate mitochondria using a Tissue Mitochondria Isolation Kit (Beyotime; Shanghai, China) according to the manufacturer's instructions. For mitochondrial morphology analysis, liver tissues (2 mm × 2 mm) were stripped within 1-3 min and immediately placed into electron microscope fixing solution. Tissues were fixed at room temperature for 2 h and then transferred to 4°C for 24 h. TEM images were captured on TECNAI G2 20 TWIN (FEI) (performed by Servicebio Inc.). Mitochondrial abnormalities were defined as the presence of one of the following morphological signs: membrane rupture, size enlargement, and cristae irregularity. For mitochondrial membrane potential analysis, freshly isolated hepatocytes were resuspended in 100 μl prewarmed with PBS, and then stained with a MitoProbeTM JC-1 Assay Kit (10 μM; Invitrogen) at 37°C for 20 min. Then, the cells were washed with PBS and stained with 10 μg/ml DAPI prior to flow cytometry analysis.

Serum levels of IL-6 and lipase

Serum was collected from mice with the indicated treatment, and the levels of interleukin-6 (IL-6; BioLegend) and lipase (Jiancheng, Nanjing, China) were determined according to the manufacturer's instructions.

Chemotaxis assay

Monocyte chemotaxis assays were performed in 24-well plates containing Transwell inserts with 5.0 mm pores as previously described. Briefly, BMDMs were resuspended in prewarmed chemotaxis medium (RPMI 1640 containing 0.5% bovine serum albumin) and incubated at 37°C for 1 h. CCL2 (100 ng/ml, BioLegend) was added to the lower part of a Boyden chamber, and BMDMs were treated with βOHB (10 mM) placed in the upper chamber. After 3 h of incubation, cells that had migrated through the membrane were collected and aliquoted for cell number and phenotype analysis by flow cytometry (BD Biosciences). Precision Count Beads (BioLegend) were spiked in each sample to determine the total number of migrated cells. Inflammatory monocytes were gated as the $CD11b^{+}Ly6C^{hi}$ population.

Flow cytometry

For cell surface staining, the single-cell suspensions were incubated with the antibody cocktails for 20 min at 4°C. For intracellular cytokine staining, immediately after isolation, BMDMs were cultured in RPMI complete medium and stimulated with LPS (100 ng/ml) and brefeldin A (10 μg/ml, BioLegend) for 4 h. The cells were washed and stained with surface markers and then fixed and permeabilised using the Foxp3 Transcription Factor Staining Buffer Set (Invitrogen) following by cytokine antibodies incubation for 20 min at 4°C. Antibodies are from BioLegend unless indicated APC- conjugated CD45.2 (104), PE-cy7-conjugated CD4 (RM4-5), Percp5.5-conjugated CD11b (M1/70), BV42-conjugated F4/80 (BM8), APC-cy7-conjugated CD11c (N418), AF488-conjugated CD206 (C068C2), PB-conjugated Ly-6C (HK1.4), PE-conjugated Ly6G (1A8), and PE-conjugated TNFα (BD Biosciences). Data were obtained on a Fortessa LSRII (BD Biosciences) and analysed using FlowJo software (Tree Star, OR, USA).

Immunoblotting and immunoprecipitation

Mouse liver tissues or cells were homogenised in lysis buffer (60 mM pH 6.8 Tris-HCl, 25% glycerol, 2% SDS, 5% β-mercaptoethanol, and 19% (vol/vol) ddH2O were supplemented with 1 mM PMSF (Yeason, Shanghai, China) and protease inhibitor cocktail (MedChem Express). HMGCS2 (Santa Cruz), Sirtuin 3 (SIRT3; Proteintech, Wuhan, China), CPT1a (Proteintech), CPT2 (Proteintech), COXIV (Proteintech), p-p65 (Biological Reagents Company Limited; Shanghai, China), p65 (Biological Reagents Company Limited), ac-p65 (Biological Reagents Company Limited), ac-H3 (Active Motif; Shanghai, China), ac-H4 (Active Motif), and β-actin (Proteintech) were used for Western blotting. For immunoprecipitation, cells or mitochondrial lysates were immunoprecipitated with the indicated antibody at 4°C for 4 h, and then protein A/G Agarose was added at room temperature for 2 h. The beads were washed with ice-cold lysis buffer and boiled in SDS-PAGE loading buffer for 5 min before electrophoresis.

Chromatin immunoprecipitation

Chromatin immunoprecipitation (ChIP) analyses were performed with ac-H3 and ac-H4 antibodies and a ChIP Assay Kit (Sigma Aldrich) according to the manufacturer's instructions. Acetylation of H3 and H4 enrichment was quantified using quantitative RT-PCR and expressed as fold change to input. The primers for ChIP-qPCR are listed as follows:

Edn1-ChIP-F: GACGGAATCTTTCTCACCTCA
ChIP-R: CACTCTTCGCTCTTGAATCCC

Il12a-ChIP-F: GACGCACTTGTCCTTGAGATGTAG
ChIP-R: GGCTGTTGGAACGCTGACCTT

NOS2-ChIP2-F: CAGGGTCACAACTTTACAGGG
ChIP2-R: TCCGTGGAGTGAACAAGACCC

Quantitative PCR

To quantify messenger RNA transcript abundance, RNA was extracted using TRIzol Reagent (Invitrogen) followed by reverse transcription using a High Capacity cDNA RT Kit (Invitrogen). The target cDNA was amplified by RT-PCR with SYBR Green (Roche) and the results were normalised to the housekeeping gene *Gapdh* (ΔCt). Relative expression was then analysed using the $2^{-\Delta Ct}$ method and the relative fold change was plotted with the control samples as 1.0. The sequences of the primers are listed as follows:

Hmgcs2 forward: 5'-GAAGAGAGCGATGCAGGAAAC-3', reverse: 5'- GTCCACATATTGGGCTGGAAA-3';

Bdh1 forward: 5'- ACAAGACACACGCTGTTGTTT-3', reverse: 5'-CTCTTCAAGCTGTCCAGTTCC -3';

Cpt1a forward: 5'-CTCCGCCTGAGCCATGAAG -3', reverse: 5'- CACCAGTGATGATGCCATTCT-3';

Tnfa forward: 5'- CCAAAGGGATGAGAAGTTCC -3', reverse: 5'-CTCCACTTGGTGGTTTGCTA-3';

Nos2 forward: 5'- GTTCTCAGCCCAACAATACAAGA-3', reverse: 5'- GTGGACGGGTCGATGTCAC-3';

Il6 forward: 5'- CCACGGCCTTCCCTACTTC-3', reverse: 5'- TTGGGAGTGGTATCCTCTGTGA-3';

Il12p40 forward: 5'- GTGGAGTGCCAGGAGGACA-3', reverse: 5'- TCTTGGGTGGGTCAGGTTT-3';

Gapdh forward: 5'- TGTGTCCGTCGTGGATCTGA-3', reverse: 5'- CCTGCTTCACCACCTTCTTGA-3';

Il12a forward: 5'- CTGTGCCTTGGTAGCATCTATG-3', reverse: 5'- CTGTGCCTTGGTAGCATCTATG-3';
Il12b forward: 5'- TGGTTTGCCATCGTTTTGCTG-3', reverse: 5'- ACAGGTGAGGTTCACTGTTTCT-3';
Edn1 forward: 5'- GCACCGGAGCTGAGAATGG-3', reverse: 5'- GTGGCAGAAGTAGACACACTC-3';
Il15 forward: 5'- ACATCCATCTCGTGCTACTTGT-3', reverse: 5'- GCCTCTGTTTTAGGGAGACCT-3';
Il27 forward: 5'- CTGTTGCTGCTACCCTTGCTT-3', reverse: 5'- CACTCCTGGCAATCGAGATTC-3';
Csf1 forward: 5'- GGCTTGGCTTGGGATGATTCT-3', reverse: 5'- GAGGGTCTGGCAGGTACTC-3';
Csf2 forward: 5'- GGCCTTGGAAGCATGTAGAGG-3', reverse: 5'- GGAGAACTCGTTAGAGACGACTT-3';
Cited2 forward: 5'- CGCCAGGTTTAACAACTCCCA-3', reverse: 5'- TGCTGGTTTGTCCCGTTCAT-3';
Cebpd forward: 5'- CGACTTCAGCGCCTACATTGA-3', reverse: 5'- CTAGCGACAGACCCCACAC-3';
Pik2 forward: 5'- CCTGCGGACTATCACCTACCA-3', reverse: 5'- CTGCCCATCTTCAGAAGGCT-3';
Ncor2 forward: 5'- AACACCACCCCCGTGACTA-3', reverse: 5'- CTGAGACCGTTCACTCCCA-3';
Notch1 forward: 5'- CCCTTGCTCTGCCTAACGC-3', reverse: 5'- GGAGTCCTGGCATCGTTGG-3';
Numbl forward: 5'- GCAGGCACCATGAA-CAAGTTA-3', reverse: 5'- TCTTCACAAACGTG-CATTCCC-3';
Stat1 forward: 5'-CGGAGTCGGAGGCCCTAAT-3', reverse: 5'-ACAGCAGGTGCTTCTTAATGAG-3';
Egr2 forward: 5'- GCCAAGGCCGTAGACAAAATC-3', reverse: 5'- CCACTCCGTTCATCTGGTCA-3';
Klf10 forward: 5'- ATGCTCAACTTCGGCGCTT-3', reverse: 5'- CGCTTCCACCGCTTCAAAG-3';
Nr4a1 forward: 5'- TTGAGTTCGGCAAGCCTACC-3', reverse: 5'- GTGTACCCGTCCATGAAGGTG-3';
Smad6 forward: 5'- GCAACCCCTACCACTTCAGC-3', reverse: 5'- GTGGCTTGTACTGGTCAGGAG-3';
Bcl6 forward: 5'- CCGGCACGCTAGTGATGTT-3', reverse: 5'- TGTCTTATGGGCTCTAAACTGCT-3';
Rara forward: 5'- ATGTACGAGAGTGTG-GAAGTCG-3', reverse: 5'- ACAGGCCCGGTTCTGGTTA-3'.

Statistical analysis

Statistical analyses were performed using GraphPad Prism Software. Continuous variables are expressed as the mean ± SD, mean ± SEM or median with 25th–75th percentile (or range). They were compared by one-way ANOVA (multiple groups) and unpaired Student's *t* test (2 groups) if they were normal distributed. Otherwise, they were compared by Kruskal-Wallis *H* test (3 groups) and Mann-Whitney *U* test (2 groups). Categorical data are presented as numbers with percentages and were compared by means of χ^2 or Fisher's exact tests. In all analyses, a p value of < 0.05 was considered to be statistically significant.

Role of the funding source

The funders have no role in the study design, data collection, data analysis, interpretation or report writing.

Results

Hepatic FAO and ketogenesis processes are activated in both human and experimental AP

Little is known about the contribution of endogenous metabolic processes/metabolites to the pathogenesis of AP. Given the central role of the liver in metabolism, we explored the alteration of hepatic metabolites during AP. We first determined circulating βOHB levels in a previously reported cohort (Cohort 1, n = 41),[26] which included AP patients and healthy controls (Figure 1a, Table S1). We found that circulating βOHB levels on the 2nd day of admission (at approximately 60 h from pain onset) were elevated in patients with mild AP (MAP; no local or systemic complication) and moderately severe AP (MSAP; local complication without persistent organ failure), but only the levels in MAP were of statistical significance when compared to healthy controls and SAP (Figure 1a). To confirm the above findings, sera from an independent validation cohort (cohort 2, n = 211; Figure 1b and Table S2) were used to detect the dynamic levels of circulating βOHB. Compared to day 1 (median 18 h from pain onset) of hospital admission, the circulating βOHB levels peaked on day 3, and the levels were significantly higher in patients with non-SAP (MAP and MSAP) than in those with SAP (Figure 1b). Furthermore, the circulating βOHB levels were similar between patients with or without admission hypertriglyceridaemia (≥ 11.3 mmol/l or 1000 mg/dl) with different severities on each day observed (Table S3).

To explore potential mechanism explaining these findings in AP patients, we generated experimental AP model using the cholecystokinin analog caerulein in mice by adjusting injection regimens to establish CER-AP (Cer*7) and CER-AP (Cer*12) (Figure 1c). Here, we deliberately avoided using AP models (i.e., bile acid-induced) that might have direct effects on liver injury. In line with previous reports,[29,30] mice with CER-AP (Cer*12) had marked pancreatic necrosis and significant lung and liver injuries compared with those with CER-AP (Cer*7), which had restrained local and systemic damages (Fig. S1a–f). Moreover, more accumulated lipid droplets in hepatocytes and accelerated lipolysis in abdominal fat were also observed in CER-AP (Cer*12) (Fig. S1 g, h). Consistent with findings from AP patients, elevated serum βOHB was noted in CER-AP (Cer*7) mice, but not in CER-AP (Cer*12) mice at 24 h post disease induction (Figure 1c). More interestingly, we found that serum βOHB was elevated as early as 6 h after the first caerulein injection (Figure 1d), indicating its role in the early pathogenesis of AP.

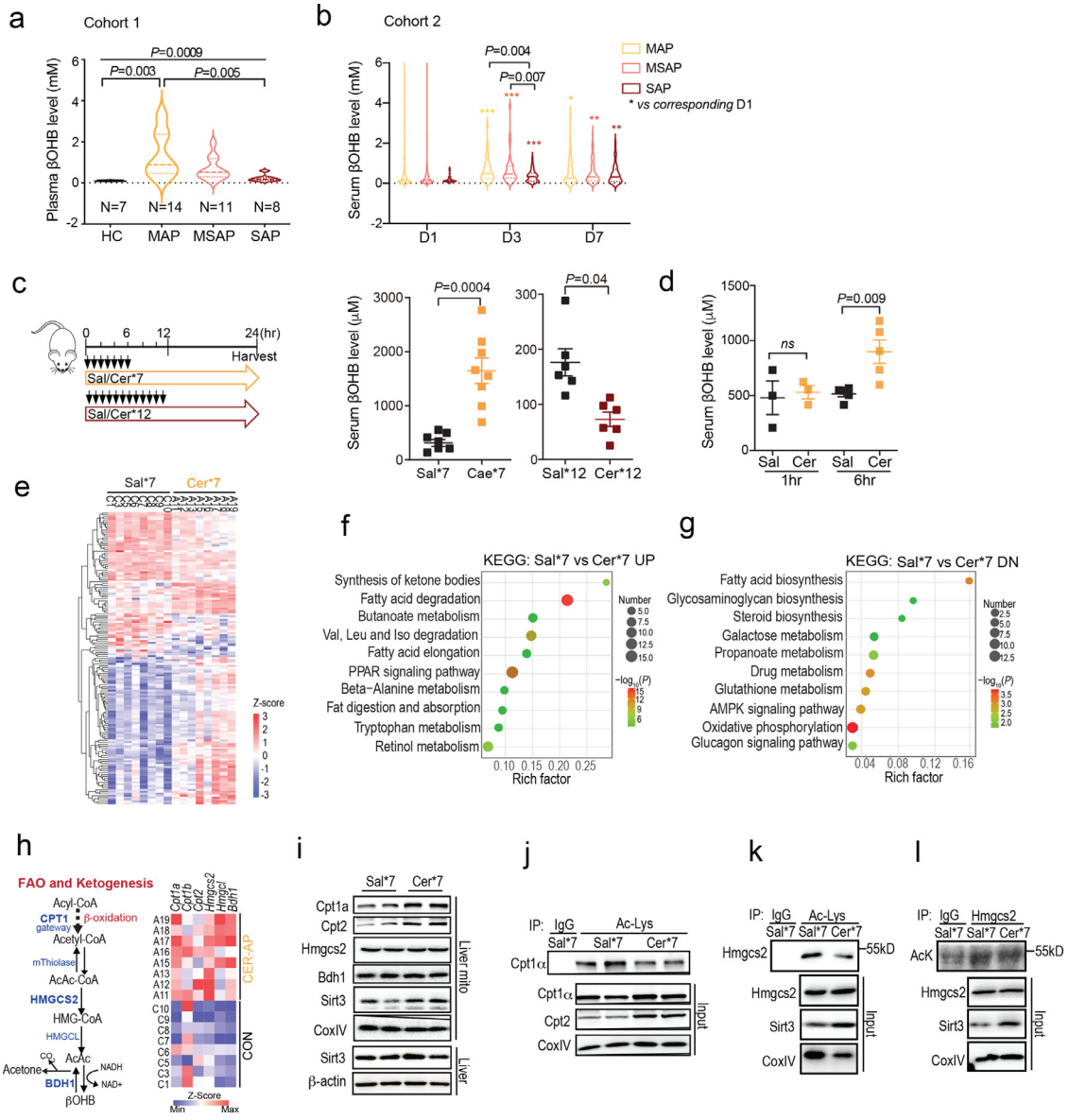

Figure 1. Hepatic FAO and ketogenesis processes are activated in AP, (a) Plasma βOHB levels of patients from cohort 1 on the second day of admission. Healthy controls (HC, n = 8) and patients with mild AP (MAP, n = 14), moderately severe AP (MSAP, n = 11), and severe AP (SAP, n = 8). Values are the mean ± SEM. (b) Serum βOHB levels of MAP (n = 85), MSAP (n = 81), and SAP (n = 45) from cohort 2 on day 1 (D1), day 3 (D3) and day 7 (D7) after the onset of disease. Values are the mean ± SEM. *p < 0.05, **p < 0.01, ***p < 0.001. (c) Serum βOHB levels in CER-AP (Cer*7) and CER-AP (Cer*12) mice using Sal*7 and Sal*12 as respective controls at 24 h after the first caerulein/saline injection (mean ± SEM, n=6-8 / group). (d) Serum βOHB levels at 1 h and 6 h after first injection (mean ± SEM, n = 3-5 / group). (e) Hepatic transcriptome analysis of differentially expressed genes (DEGs) from the indicated mice (n = 8 / group). (f-g) KEGG pathway enrichment analyses. UP, upregulated; DN, downregulated. (h) Expression of fatty acid β-oxidation (FAO)- and ketogenesis-related genes according to hepatic transcriptome data. (i) Immunoblotting of the indicated proteins in the mitochondria (mito) and whole tissues of livers. (g-l) Liver mitochondrial extracts from the indicated mice were immunoprecipitated with antibodies specific for acetyl-lysine (Ac-Lys) or Hmgcs2 and then immunoblotted with the indicated antibodies.

To comprehensively understand the impact of AP on hepatic metabolism, we compared the hepatic transcriptome profile between CER-AP (Cer*7) and control (Sal*7) mice (Figure 1e). Of note, the upregulated DEGs were linked to the synthesis of ketone bodies (ketogenesis) and fatty acid degradation (Figure 1f), while the downregulated DEGs were involved in fatty acid biosynthesis (Figure 1g). As the key rate-limiting enzyme of FAO, CPT1 converts LC acyl-CoA to its corresponding LC acyl-carnitine for transport into

mitochondria.[36] HMGCS2, a rate-limiting enzyme of ketogenesis, is nearly exclusively localised to the liver and catalyses AcAc-CoA to generate HMG-CoA. Next, HMG-CoA lyase (HMGCL) cleaves HMG-CoA to liberate AcAc, which is then reduced to βOHB by βOHB dehydrogenase (BDH1).[37] Intriguingly, both RNA-seq and qPCR analyses confirmed that the mRNA levels of *Cpt1a, Hmgcs2*, and *Bdh1* were markedly increased in the CER-AP (Cer*7) group (Figure. 1h, S1l). While the protein level of Cpt1α was slightly upregulated, Hmgcs2 had no significant difference in the liver mitochondria between the two groups (Figure 1i). In addition to transcriptional regulation, growing evidence has shown the regulation of CPT1α and HMGCS2 activities by protein deacetylation.[38,39] SIRT3, which shuttles from the cytoplasm to mitochondria, has been identified as the major deacetylase of CPT1α and HMGCS2.[39–41] Here we found the Sirt3 expression in liver mitochondria was upregulated (Figure 1i) and acetylation of Cpt1α and Hmgcs2 was decreased in CER-AP (Cer*7) compared with the control group (Figure 1j–l), implying elevated activities of Cpt1α and Hmgcs2 in the liver of the experimental AP. Taken together, these results indicate that hepatic FAO and ketogenesis are activated in experimental AP, and two main questions are raised: 1) Why is there a difference in hepatic ketogenesis between CER-AP (Cer*7) and CER-AP (Cer*12)? 2) What is the function of elevated FAO-ketogenesis in AP?

Liver LC-FAO impairment and mitochondrial dysfunction lead to insufficient ketogenesis in more severe AP

To further understand the difference in hepatic ketogenesis between CER-AP (Cer*7) and CER-AP (Cer*12), we analysed the unique DEGs comparing Cer*12 vs Sal*12 and Cer*7 vs Sal*7. The unique upregulated DEGs in CER-AP (Cer*12) were mainly related to the inflammatory response, innate immune response, endoplasmic reticulum (ER) unfolded, and tumour necrosis factor (TNF) signalling, suggestive of greatly enhanced hepatic inflammation and ER stress (Figure. 2a, S2a, b). The unique downregulated DEGs in CER-AP (Cer*12) mainly linked to oxidation reduction, FAO, and TCA processes, indicating impaired mitochondrial energy metabolism (Figure 2b). Consistently, the genes encoding the respiratory chain complexes were largely downregulated in the livers of CER-AP (Cer*12) (Fig. S2c, d). By transmission electron microscopy (TEM) analysis, we found that both the number of mitochondria and the ratio of abnormal mitochondria increased in the livers of CER-AP (Cer*12) mice (Figure 2c). The impaired function and altered morphology of mitochondria indicated that the livers from CER-AP (Cer*12) were under pronounced metabolic stress, as evidenced by increased lipid droplets in hepatocytes (Fig. S1 g, h).

Furthermore, by comparing the relative levels of liver metabolites via targeted metabolome analysis, we found that the levels of total fatty acids and total carnitines were dramatically increased, while total carbohydrate levels were further decreased in CER-AP (Cer*12) compared with CER-AP (Cer*7) (Figure 2d). KEGG pathway enrichment analysis showed that the altered hepatic metabolites in CER-AP (Cer*12) were predominantly related to LC-FAO and carnitine synthesis (Figure 2e). Carnitine is only essential for transferring LC fatty acids across the inner mitochondrial membrane for subsequent β-oxidation.[42] As expected, LC acyl-carnitines (C16:0, C18:0, C18:1, and C18:2) only increased dramatically in the livers of CER-AP (Cer*12) (Figure 2f). Consistently, the acetylation of CPT1α was reduced in the livers of CER-AP (Cer*7) but increased in the CER-AP (Cer*12), in comparison with the corresponding controls (Figure 2g). Herein, these findings are indicative of defective LC-FAO in the liver of CER-AP (Cer*12) mice, further leading to insufficient ketogenesis, accumulation of lipotoxic metabolites, and even liver injury.

Suppression of endogenous FAO-ketogenesis aggravates the severity of AP

Next, we explored the role of endogenous FAO and ketogenesis in the pathogenesis of experimental AP. First, etomoxir, the antagonist of CPT1α, was administrated 1 h prior to the first caerulein injection and it almost abolished the elevation of serum βOHB in the CER-AP (Cer*7) mice (Figure 3a). Etomoxir markedly increased the overall pancreas histopathological score (Figure 3b), as well as elevated serum amylase, IL-6 and alanine aminotransferase (ALT) levels of the CER-AP (Figure 3c–e), indicating augmented pancreatic and liver injuries post FAO/ketogenesis blockage. We further assessed the impact of HMGCS2 blockade on the severity of CER-AP (Cer*7). To this end, mice first received tail vein injection of lentivirus expressing validated sh-Hmgcs2 or scrambled shRNA (sh-Con) as a control, at three weeks later followed by CER-AP induction (Figure 3f). In the sh-Hmgcs2 versus sh-Con comparison, knocking down *Hmgcs2* resulted in decreased expression of liver Hmgcs2 (Figure 3f) and circulating βOHB levels (Figure 3g) at 24 h after CER-AP induction. Consistent with findings from etomoxir administration, sh-Hmgcs2 markedly exacerbated the overall pancreas histopathological score (Figure 3h), accompanied by an increased proportion of TNFα$^+$ macrophages in the pancreas (Figure 3i). Together, the above results suggest that blockage of endogenous hepatic FAO/ketogenesis processes during AP exacerbated the severity of disease.

Exogenous supplementation with βOHB alleviates the severity of AP

Next, we investigated whether supplementation with exogenous ketone body was able to protect against AP.

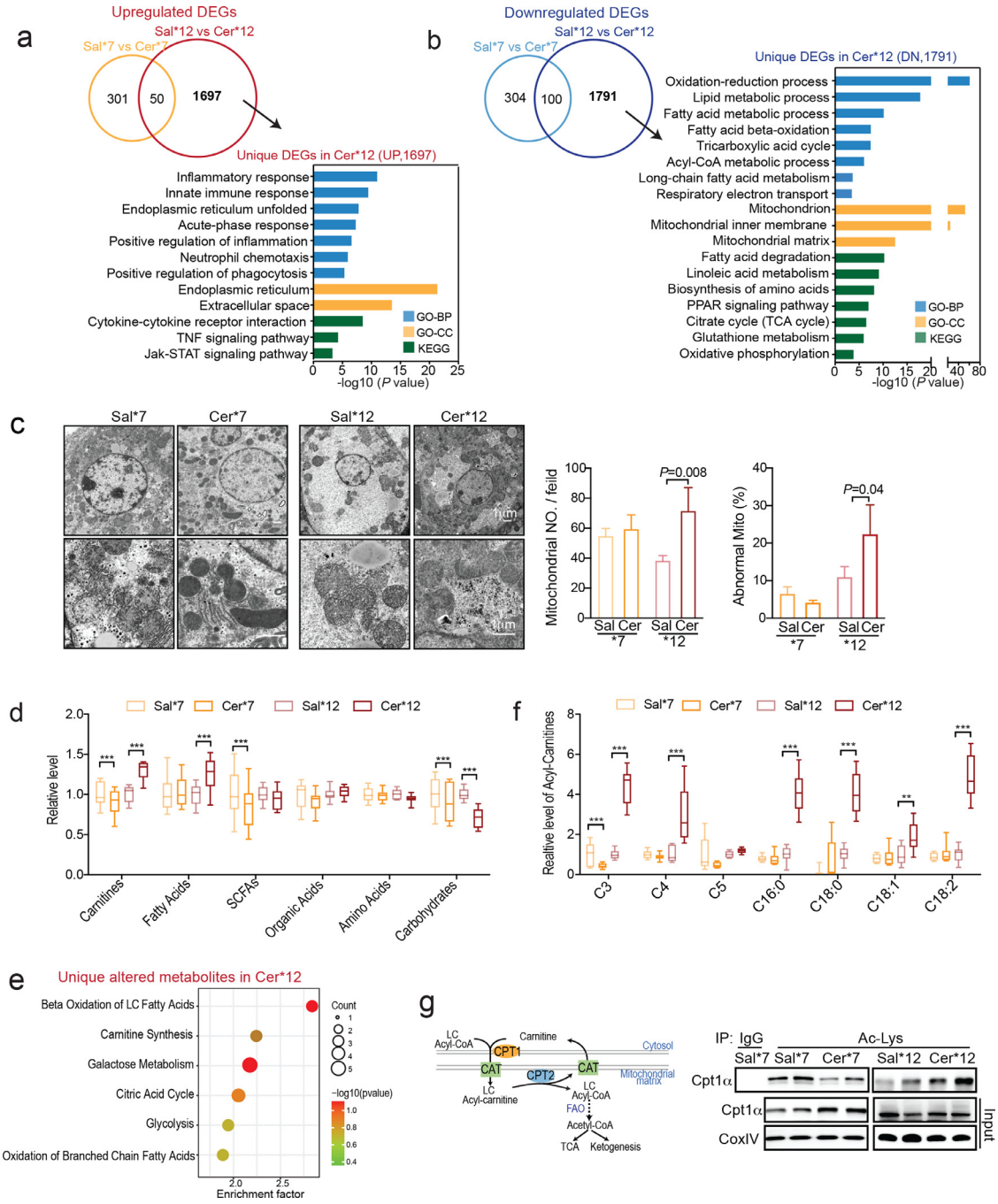

Figure 2. Liver LC-FAO impairment and mitochondrial dysfunction lead to insufficient ketogenesis in more server AP, (a, b) Venn and KEGG/GO analyses of unique upregulated (A) or downregulated (B) differentially expressed genes (DEGs; FC $>$ 1.5, p $<$ 0.05) in the livers of CER-AP (Cer*12) compared to control livers (Sal*12). (c) Representative TEM images of the liver mitochondria. Semi-quantitative assessment of mitochondria number per field, and the percentage of abnormal mitochondria in the indicated groups (n = 3, mean $\pm$ SEM). (d) Metabolomic analysis of the livers from CER-AP (Cer*7), CER-AP (Cer*12) and their respective control mice (n = 6−8 / group). Relative levels of the indicated metabolite categories. SCFAs, short-chain fatty acids. (e) KEGG pathway enrichment analysis of unique altered metabolites in CER-AP (Cer*12) mice. (f) Short- and long-chain acylcarnitine profiles in the livers of the indicated groups. (g) Acylated Cpt1α (Ac-Cpt1α) levels in the livers of mitochondria were determined by immunoprecipitation from the indicated group. *p $<$ 0.05, **p $<$ 0.01, ***p $<$ 0.001. Data are presented as the median with minimum and maximum values in (d and f).

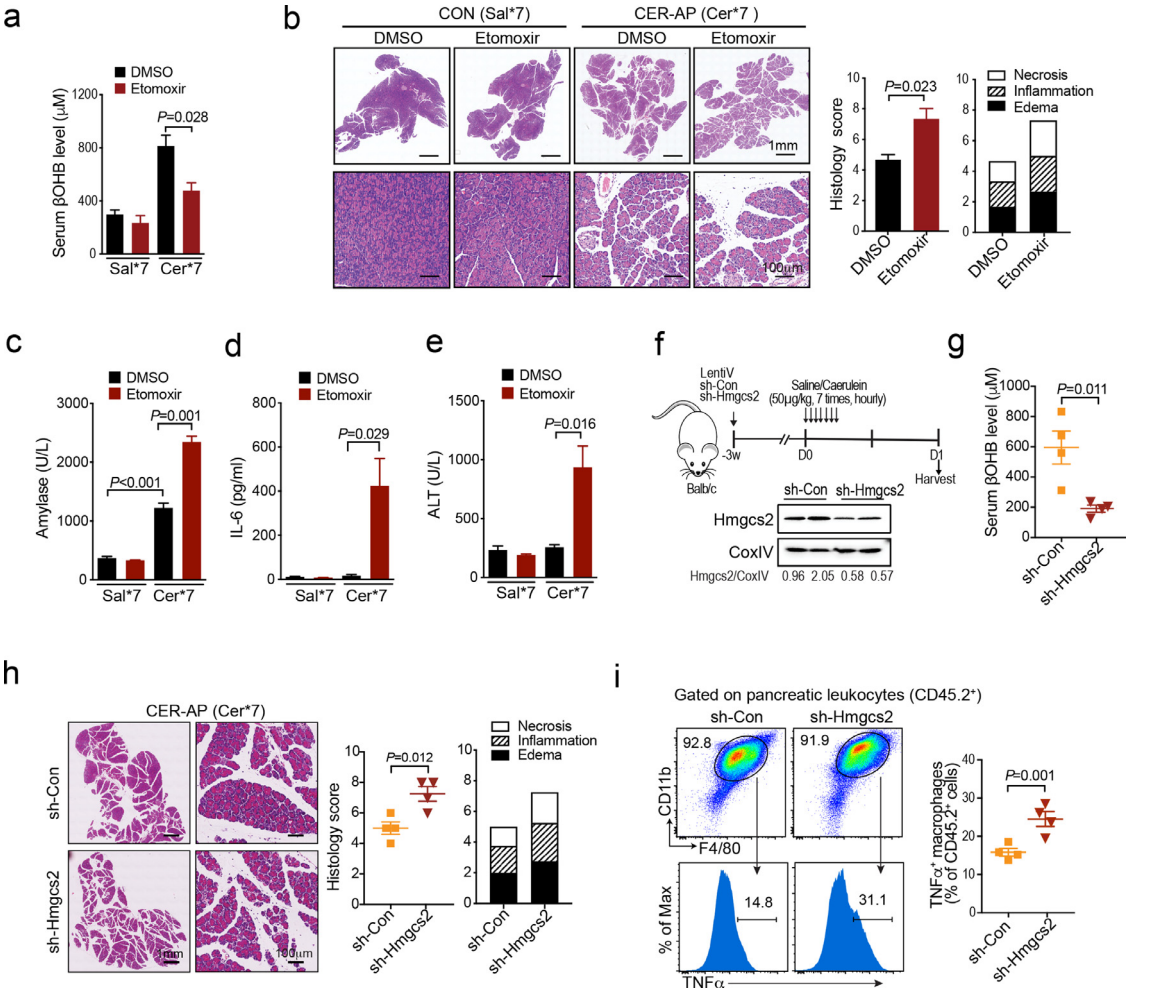

Figure 3. Suppression of endogenous FAO and ketogenesis worsens AP, (a–e) Mice were i.p. injected with DMSO and etomoxir (20 mg/kg) 1 h prior to first caerulein injection (Cer*7, 50 μg/kg) and were harvested at 24 h (n = 3 / group). (a) Serum βOHB levels from the indicated groups. (b) Representative pancreatic H&E images and histology score. (c-d) Serum levels of amylase (c), IL-6 (d) and ALT (e) from the indicated groups. (f–i) sh-Hmgcs2 or sh-Con wrapped with lentivirus was i.v. injected into Balb/c mice for three weeks prior to AP induction (Cer*7, 50 μg/kg, n = 4 / group). (f) Liver mitochondria HMGCS2 protein levels. (g) Serum βOHB levels. (h) Representative pancreatic H&E images and histology scores from sh-Con and sh-Hmgcs2 mice. (i) Frequency of TNFα^+ macrophages (F4/80$^+$CD11b$^+$) in pancreatic leukocytes from the indicated groups. All data are presented as the mean ± SEM.

Mice were given drinking water with or without 1,3-butanediol, the precursor of βOHB prior to induction of CER-AP (Cer*7). Here we found that 1,3-butanediol feeding for one week was able to increase the serum βOHB level of mice to 1-2 mM, within the physiological concentration range and without systemic toxicity (Figure. 4a, S3a). Moreover, 1,3-butanediol pretreatment markedly ameliorated the severity of CER-AP as evidenced by significantly reduced overall pancreas histopathological score, which predominantly attributed to necrosis and inflammation (Figure 4b). It also reduced serum amylase levels (Figure 4c), and decreased the proportion of pancreatic TNFα^+ macrophages at 24 h after the first caerulein injection (Figure 4d). More interestingly, as early as 6 h after the first caerulein injection, 1,3-butanediol pretreatment led to a decrease in the proportion of CD11b$^+$Ly6C^{hi} monocytes in total leukocytes (CD45.2$^+$) from the pancreas and circulation of CER-AP mice (Fig. S3b). To further confirm the role of dietary ketone body in the prevention of AP, the CER/LPS-SAP model mimicking septic necrotising AP was employed.[31] Similarly, 1,3-butanediol pretreatment was able to reduce the overall pancreas histopathology score (Figure 4e), lung alveolar membrane thickening (Figure 4f) and the TNFα levels of monocytes/macrophages in the pancreas, spleen, and mesenteric lymph nodes (Figure 4g).

Next, to confirm that the protective effects were mediated by elevated βOHB after 1,3-butanediol feeding, βOHB was intraperitoneally injected into mice 1 h

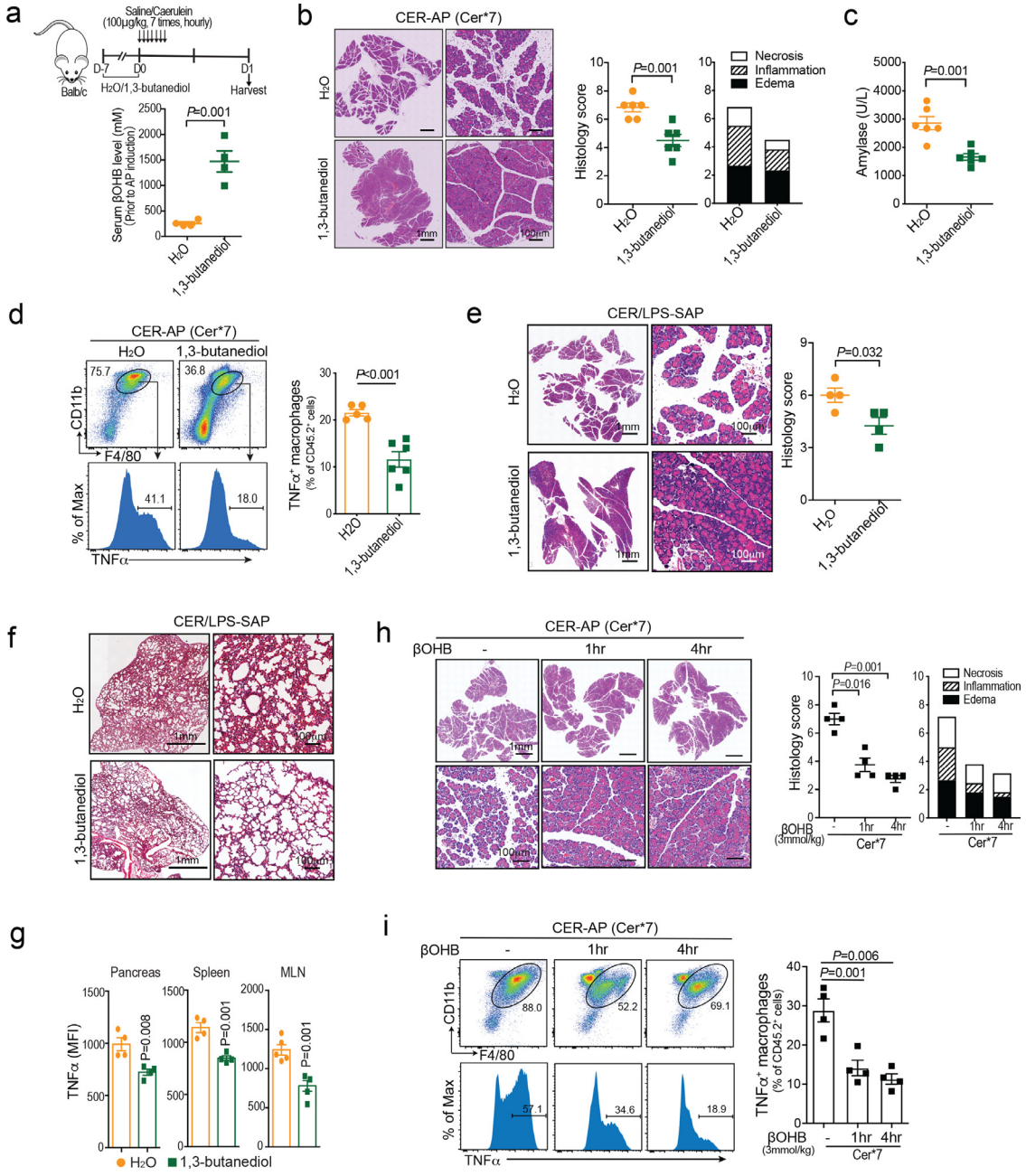

Figure 4. Exogenous supplementation with βOHB alleviates the severity of AP, (a−d) Mice were pre-fed with or without the precursor of βOHB, 1,3-butanediol , in drinking water for 1 week prior to AP induction (n = 4-6 / group). (a) Serum βOHB levels of the indicated groups prior to AP induction. (b−d) Mice were harvested at 24 h after first injection of caerulein. (b) Representative pancreatic H&E images, (c) serum amylase levels, and (d) frequency of TNFα$^+$ macrophages (F4/80$^+$CD11b$^+$) in pancreatic leukocytes for H_2O or 1,3-butanediol-treated CER-AP (Cer*7) mice. (e−g) Mice were pre-fed with or without 1,3-butanediol in drinking water for 1 week prior to CER/LPS-SAP induction. Mice were harvested at 24 h (n = 4 / group). (e) Representative pancreatic H&E images and histology scores. (f) Representative H&E images of lung from the indicated groups. (g) TNFα level (MFI) in monocytes/macrophages (CD11b$^+$) from the pancreas, spleen and mesenteric lymph nodes (MLN). (h−i) Mice were i.p. injected with βOHB (3 mmol/kg) at 1 h or 4 h post AP and were harvested at 24 h (n = 4-5 / group). (h) Representative pancreatic H&E images and histology scores (i) frequency of TNFα$^+$ macrophages (F4/80$^+$CD11b$^+$) in pancreatic leukocytes from the indicated groups. All data are presented as the mean ± SEM.

before CER-AP induction. βOHB supplementation had effects equivalent to those of 1,3-butanediol feeding in preventing AP (Fig. S3c, d). More importantly, βOHB intervention at 1 h or 4 h after CER-AP induction was also able to attenuate pancreatic injury and pancreatic macrophage activation (Figure 4h, i). Thus, all these data demonstrated that exogenous supplementation with βOHB was able to alleviate the severity of AP, indicating its potential value for preventing and treating AP.

βOHB directly restrains the activation of proinflammatory macrophages

To understand how βOHB protects against AP, we assessed its direct effects on both pancreatic acinar cell damage and proinflammatory macrophage activation *in vitro*, which are the two major events in determining the severity of AP.[6,43] First, we found that βOHB had no protective effect on pancreatic acinar cell damage triggered by caerulein. Instead, when the concentration reached 10 mM (a concentration unlikely to reach when given 1,3-butanediol feeding or βOHB supplementation *in vivo*), βOHB was slightly toxic to acinar cells, but not to macrophages (Fig. S4a, b). During AP, $CCR2^+$ proinflammatory monocytes were emigrated from the bone marrow and infiltrated the pancreas to further differentiate into proinflammatory macrophages (M1), which largely determined the severity of AP.[32] Thus, we subsequently focused on delineating the role of βOHB in macrophage activation during AP. The conditioned medium (CM) from caerulein-treated acini was collected to mimic local pancreatic macrophage activation (sterile inflammation) by damage-associated molecular patterns (DAMPs). As expected, similar to LPS, CM from injured acini was able to increase TNFα expression in murine BMDMs (Figure 5a). The activation of macrophages by acini CM (Figure 5b, c) and LPS (Figure 5d, e) was able to greatly antagonised by βOHB with synchronically downregulated mRNA levels of *Nos2, Il6, Il12b,* and *Tnfa* in BMDMs.

To comprehensively understand the mechanism by which βOHB restrains proinflammatory macrophage activation, we performed RNA-seq analysis in BMDMs treated with or without βOHB upon LPS stimulation (Figure 5f). A total of 7325 DEGs among the three groups (FC > 1.5, $p < 0.05$) were identified and we focused on two gene clusters: (1) Cluster A, 222 genes of LPS-inducible but βOHB downregulated. These genes were mostly involved in the immune response, TNF signalling, and Toll-like receptor 4 (TLR4) signalling (Figure 5g); (2) Cluster B, 537 genes of LPS-repressed but βOHB-upregulated. These genes were related to negative regulation of transcription, wound healing, negative regulation of nuclear factor kappa-B (NF-κB) signalling, and Notch signalling (Figure 5h). The most significantly altered genes of the two clusters were further validated by qPCR assay (Fig. S4c).

βOHB limits proinflammatory macrophage activation via class I HDACs

Notably, the inhibitory effect of βOHB on proinflammatory macrophage activation was independent of its known receptors HCAR2 and FFAR3 (Fig. S5a–c). Furthermore, GSEA showed that genes affected by βOHB were positively correlated with HDAC pan-inhibitor TSA upregulated signature genes in murine BMDMs (GSE22049) (Figure 6a). When applied to the GSE33162 database, the genes altered in the βOHB-treated group were positively correlated with genes that were downregulated in $Hdac3^{-/-}$ BMDMs (versus WT BMDMs) upon LPS treatment for 4 h (Figure 6b). According to the public database, HDAC1, HDAC2, and HDAC3 were the dominant isoforms of HDACs both in BMDMs and pancreatic macrophages (Fig. S5d). Next, we investigated the effect of TSA and MS-275 (HDAC1/3 inhibitor) on proinflammatory macrophage activation. As we expected, TSA or MS-275 had a similar effect as βOHB on inhibiting TNFα expression (Figure 6c), as well as *Nos2, Il6, Il12b,* and *Tnfa* mRNA expression in BMDMs (Figure 6d).

Previous studies have shown that LPS-induced histone acetylation, strongly dependent on HDAC3, also contributes to inflammatory gene expression in macrophages.[44] We confirmed that βOHB was able to decrease LPS-induced histone acetylation of the target genes (e.g., *Edn1, IL12a,* and *Nos2*) in BMDMs (Figure. 6e, S5e). The targets of HDACs are not restricted to histones, but also to non-histone proteins. Thus, we imported the genes of cluster A into Ingenuity Pathway Analysis (IPA) to further explore the key effectors of βOHB. Of note, NF-κB, which is crucial for proinflammatory macrophage activation, is the most evident pathway affected by βOHB in the context of LPS stimulation (Figure 6f). NF-κB (p65) was previously reported to be acetylated by HDACs, especially class I HDACs, involved in NF-κB-DNA binding activity and transcriptional potential.[45–47] Similar to TSA, βOHB simultaneously reduced the acetylation (K310) and phosphorylation (S536) of p65, indicating the impaired transcriptional activity of p65 upon βOHB treatment (Figure 6g).

To further prove our concept, TSA and MS-275 were used to test whether they were able to ameliorate pancreatic macrophage activation and AP severity *in vivo*. Consistent with published literature,[48,49] both TSA and MS-275, similar to βOHB, were able to protect against CER-AP (Fig. S5f). More importantly, similar to βOHB, TSA and MS-275 largely suppressed the activation of pancreatic macrophages in AP mice (Figure 6h). Collectively, these data reveal that βOHB limits proinflammatory macrophage activation via class I HDACs at both the epigenetic and transcriptional levels.

Discussion

This study advances several concepts of how endogenous liver metabolites modulate AP progression,

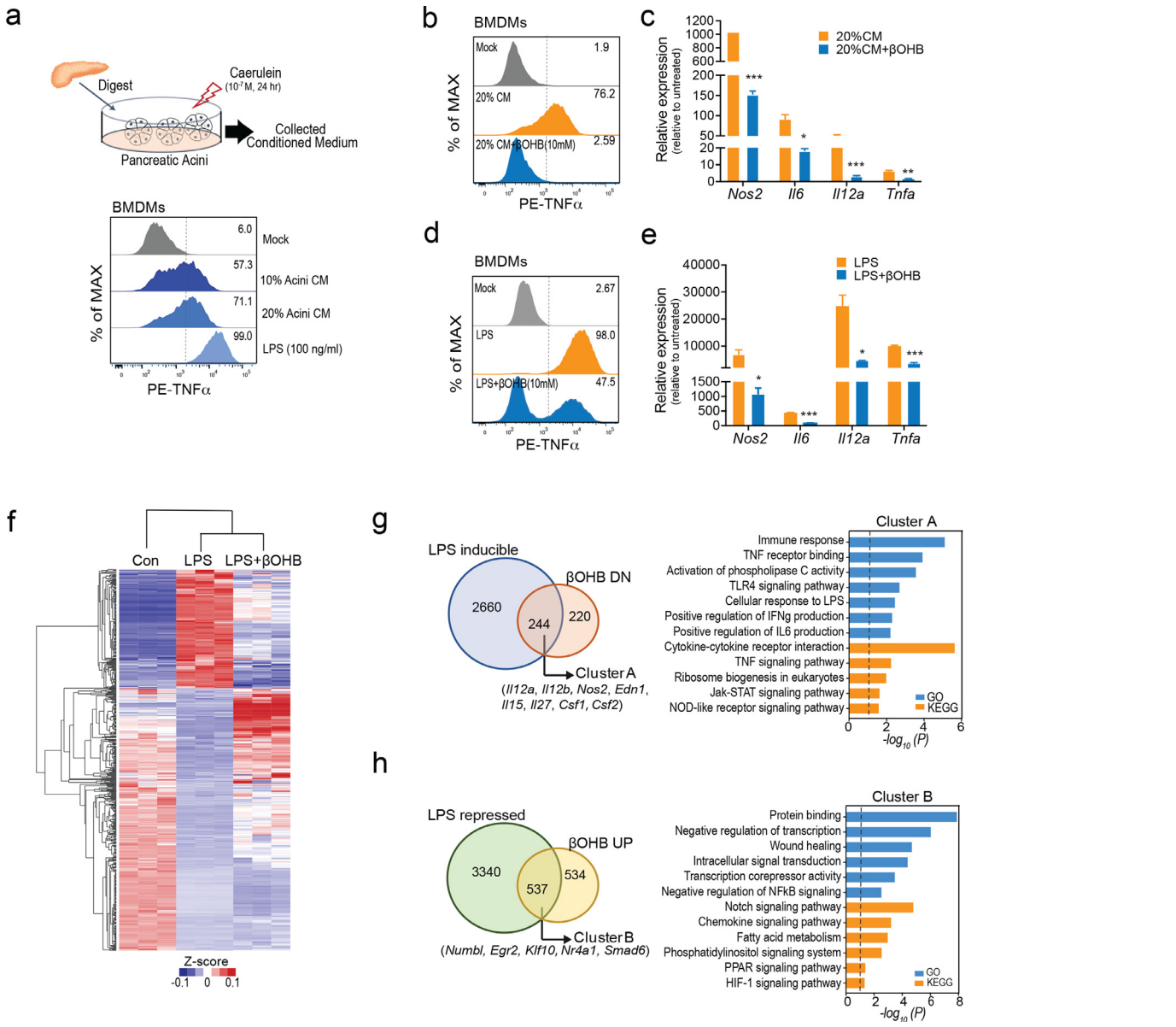

Figure 5. βOHB directly restrains the activation of proinflammatory macrophages, (a) Murine BMDMs were treated with conditioned medium collected from dead/dying acini (Acini conditioned media, CM; 10% and 20%) or LPS (100 ng/ml) for 4 h. Flow cytometry analysis of intracellular TNFα levels. (b, c) Murine BMDMs were treated with 20% Acini CM together with βOHB (10 mM) for 4 h. Flow cytometry analysis of intracellular TNFα levels and quantitative analysis of *Nos2*, *Il6*, *Il12b* and *Tnfa* mRNA expression. (d, e) Murine BMDMs were treated with LPS (100 ng/ml) together with βOHB (10 mM) for 4 h. Flow cytometry analysis of intracellular TNFα levels and quantitative analysis of the expression of the indicated genes. (f) Transcriptome analysis of murine BMDMs treated with saline (Con) or LPS with or without βOHB (10 mM) for 4 h (n = 3 / group). (g-h) Venn and KEGG / GO analyses for genes of LPS-induced but downregulated by βOHB (g, Cluster A) and LPS-repressed but upregulated by βOHB (h, Cluster B). Data are presented as the mean ± SD in bar graphs (c and e), *p < 0.05, **p < 0.01, ***p < 0.001.

namely, the CPT1α- and HMGCS2-mediated FAO-ketogenesis serves as a protective programme to limit pancreatic and systemic inflammation by inhibiting proinflammatory macrophage activation (Figure 7). Hepatic ketogenesis was largely activated (elevated circulating βOHB) in patients with MAP compared to those with SAP and this phenomenon was replicated in caerulein-induced mild (Cer*7) and severe form (Cer*12) of AP. The retarded ketogenesis in the more severe CER-AP was largely attributed to impaired mitochondrial dysfunction and defective LC-FAO in the liver. Blockade of endogenous FAO-ketogenesis

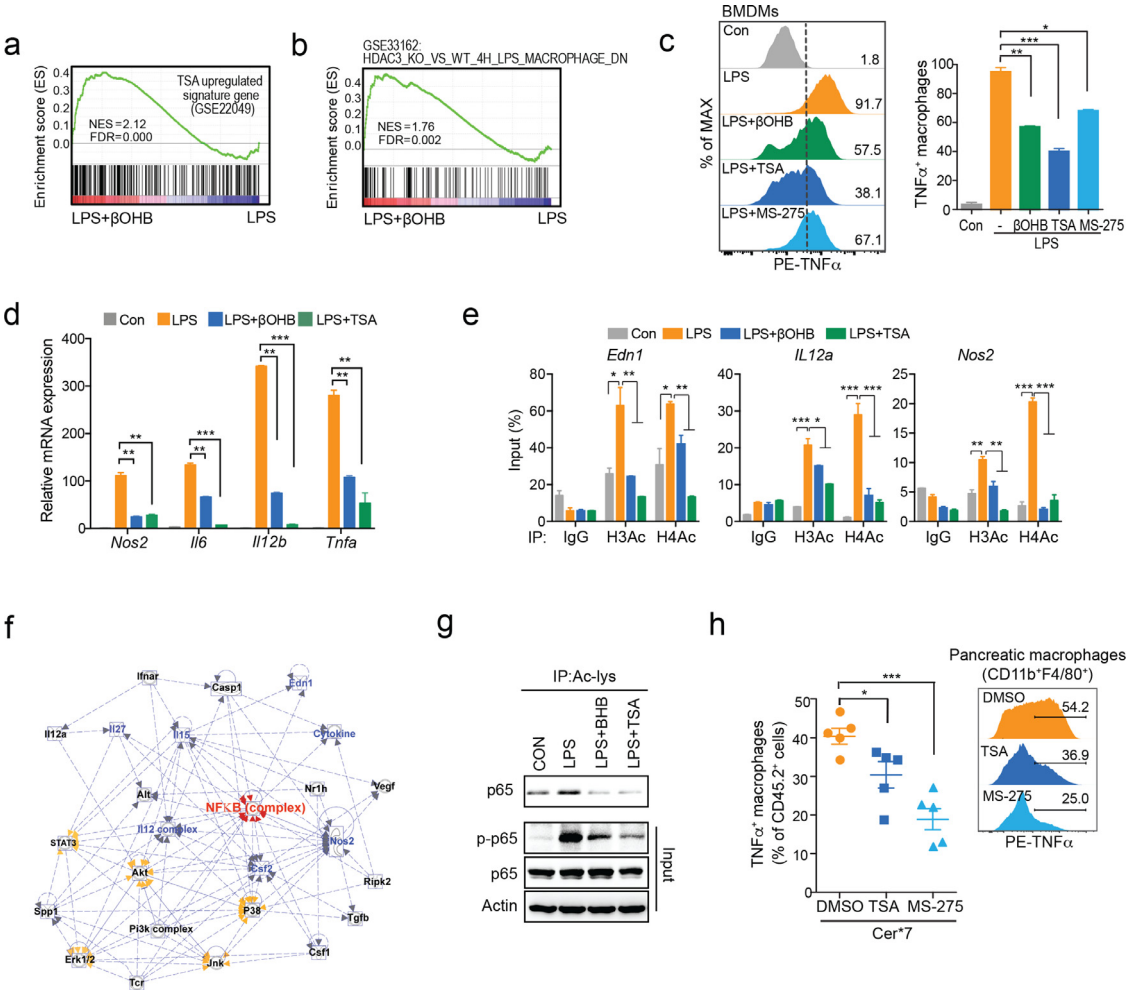

Figure 6. βOHB limits proinflammatory macrophage activation via class I HDACs, (a, b) Gene set enrichment analysis (GSEA) of gene expression in murine BMDMs are depicted. (a) Enrichment of TSA-upregulated signature genes (GSE22049) in βOHB-treated BMDMs. (b) Enrichment of HDAC3 depletion related signature genes (GES33162) in βOHB-treated BMDMs. (c, d) BMDMs treated with LPS (100 ng/ml) together with βOHB (10 mM), TSA (1 μM), or MS-275 (20 μM) for 4 h. (c) Flow cytometry analysis of intracellular TNFα levels. (d) Quantitative PCR analysis of *Nos2*, *Il6*, *Il12b*, and Tnfa mRNA expression. (e) ChIP-qPCR analysis of H3Ac and H4Ac occupancy in *Edn1*, *Il12a*, and *Nos2* loci in the indicated group, with IgG as the control. (f) Ingenuity Pathway Analysis (IPA) of genes in cluster A. (g) BMDMs were pretreated with βOHB (10 mM) or TSA (1 μM) 1 h prior to LPS (100 ng/ml) stimulation for 15 min. Acylated p65 levels were determined by immunoprecipitation, while p-p65 and total p65 were determined by immunoblotting. (h) Mice were i.p. injected with TSA (0.1 mg/kg), MS-275 (20 mg/kg) or DMSO as a control 1 h prior to the CER-AP (Cer*7) induction and were harvested at 24 h thereafter (n = 5 / group). Frequency of $TNF\alpha^+$ macrophagess ($F4/80^+CD11b^+$) in pancreatic leukocytes from the indicated groups. Data are presented as the mean ± SD in bar graphs (c−e) or the mean ± SEM in dot plots (h). *p < 0.05, **p < 0.01, ***p < 0.001

worsened, while supplementation with βOHB alleviated pancreatic inflammation, necrosis, and even organ failure in experimental AP. Furthermore, βOHB directly suppressed DAMP- and LPS-induced proinflammatory macrophage activation. These findings highlight that not only does liver metabolism is activated during AP, but it also contributes to disease progression. Therefore, targeting liver metabolism (i.e., activating the endogenous ketogenesis pathway) may provide a novel proof-of-principle strategy to tackle AP.

Self-confinement is a characteristic feature of MAP patients who recover with minimal treatment, implying that there are some endogenous protective mechanisms of AP. Systemic metabolism is commonly disrupted during AP,[11] but little is known about whether the altered endogenous metabolites participate in the development of AP. Compelling evidence has established a central role of pancreatic lipase-mediated adipose lipolysis in aggravating pancreatic damage and organ failure.[13−15] Therefore, timely elimination of NEFAs is vital

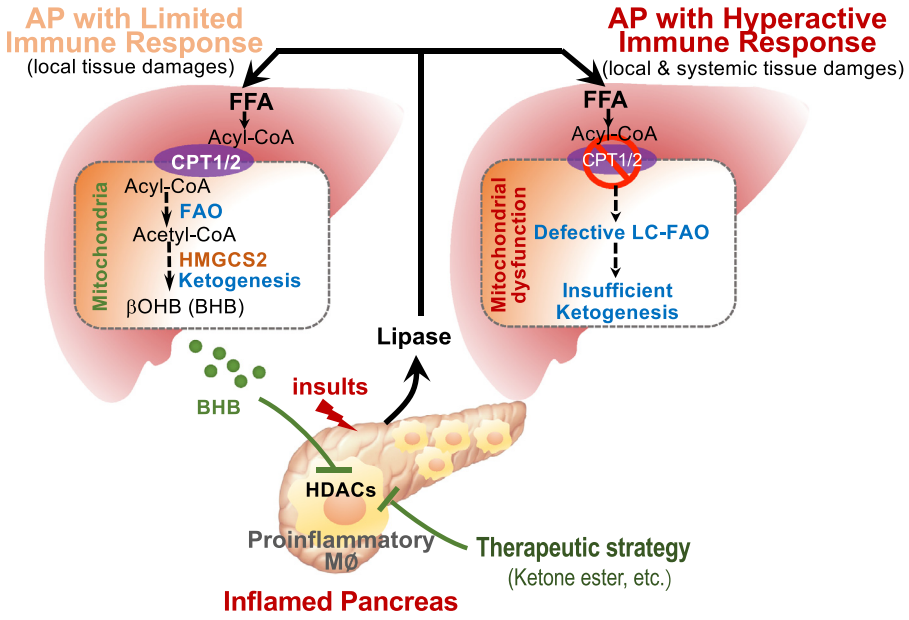

Figure 7. Schematic illustration of hepatic FAO-ketogenesis mediating the crosstalk between the inflamed pancreas and liver in acute pancreatitis.

to control disease progression. Given the central role of liver in handling fatty acids and systemic metabolism,[16] it is astonishing that how liver responds to metabolic stress during AP and how this process in turn affects disease progression remain unexplored. Recently, many studies have provided evidence that the ketogenic diet is able to protect against many inflammatory diseases via immune cells such as macrophages, and TCRγ/δ etc.[50–53] However, the endogenous role of hepatic ketogenesis in inflammatory disease also remains poorly understood. Our previous studies revealed that the severity of AP is largely determined by the innate immune response.[6] Here, we first revealed that endogenous hepatic FAO and ketogenesis act as a positive mechanism to mediate a crosstalk between the liver and inflamed pancreas in limiting disease severity.

In our study, we found that the active response of FAO and ketogenesis in milder AP was diminished in the more severe form of both human and experimental AP. Impaired mitochondrial energy metabolism was associated with enhanced lipid droplet formation, inflammation, and ER stress in livers from CER-AP (Cer*12) mice. These findings are in line with previous reports that mitochondrial dysfunction with abolished energy metabolism was a key feature for increased AP severity which was observed in pancreas, intestine, lung, and peripheral blood mononuclear cells.[54–57] Previous studies have reported that inflammation-induced ER stress and mitochondrial dysfunction can establish a vicious cycle.[58] Herein, our findings imply a vicious cycle among inflammation, mitochondrial dysfunction, and ER stress in the livers of CER-AP (Cer*12), leading to impaired FAO and ketogenesis, accumulation of lipid droplets, and profound liver inflammation and injury. Notably, to avoid direct effects of the model on the liver, we generated Cer*12 as a more severe AP model. Mice with Cer*12 exhibits local and systemic tissue damage and inflammation, even though it is not a typical SAP models with a certain rate of mortality. We speculate that mitochondrial dysfunction and impaired FAO-ketogenesis of liver would be even worse in more severe AP models (SAP) or clinical patients with SAP, which requires further investigation.

With the prevalence of metabolic syndrome worldwide,[59] AP patients are often accompanied with comorbidities associated with non-alcoholic fatty liver diseases. Recent evidence suggests that the presence of comorbid liver metabolic syndrome predisposes AP patients to SAP and higher mortality.[60–62] In addition, hypertriglyceridaemia is a well-established metabolic disorder and increasing aetiology for AP that is more virulent than other aetiologies.[63] However, as a metabolic hub organ, the liver is common albeit overlooked in current experimental and human AP. The underlying molecular mechanisms between metabolic disorders and AP remain poorly understood. Our study may provide an explanation of how fatty acid metabolism dysfunction affects the severity and outcomes of patients with AP. Thus, the liver status of AP patients with symptoms of metabolic disorders (primary or secondary) needs to be closely monitored. Moreover, we found that circulating βOHB levels were not significantly different between patients with or without hypertriglyceridaemia of different severities. It is of particular note that the dramatic elevation of ketone bodies during diabetic ketoacidosis ($\geq$3 mmol/l) has a fundamental

difference to the increased ketone bodies during AP.[64] The elevated circulating βOHB levels in AP patients rarely exceed 3 mmol/l, while in SAP patients the levels are even lower. Concomitant diabetic ketoacidosis and AP events are very rare and it is easy to rule out patients with diabetic ketogenesis if there is a randomised trial testing the safety and efficacy of ketone bodies in treating AP patients. In our study, patients with pre-existing diabetes were excluded, further clarifying our findings.

Noteworthy, current treatment of AP is largely supportive[65] with over 84 targeted pharmacological therapy randomised trials failing to show efficacy,[66] and there is a pressing need for a new avenue for this devastating disease. Although mild AP (accounting for 80% of total AP cases) is self-limited, the average hospital stay is approximately one week. Therefore, treating mild AP has big socioeconomic impact by accelerating the oral refeeding time and shortening the length of hospital stay. In addition, predicting the course of AP patients on admission is of great importance. Our study showed that both pretreatment with βOHB precursor alleviated experimental AP in both sterile and septic models. This was strengthened by the fact that βOHB intervention at 1 h and 4 h after disease induction both significantly improved pancreatic injury of CER-AP, highlighting its potential value for preventing and treating AP, which may warrant clinical trials. It has been reported that ketone monoesters are safe and well-tolerated in healthy volunteers even for prolonged administration. For prevention and intervention applications, patients before endoscopic retrograde cholangiopancreatography, or AP patients with metabolic syndrome may benefit from the administration of ketone monoesters. Of note, our proof-of-concept therapeutic potential for βOHB would not apply to AP patients who have pre-existing diabetes.[67] Moreover, when considering a boosting ketogenesis strategy for AP, we need to rule out the possibility of using a ketone diet (high fat and low carbohydrates) for patients who have existing metabolic syndrome at baseline.

Contributors

Conceptualisation, L.Z. and J.X.; Methodology, L.Z., J. S., X.Y., S.L., N.N., X.S., D.D., W.Y., P.L., and G.L.; Clinical data acquisition and interpretation, S.L., N.S., L.Y., and W.H.; Formal Analysis, J.X., L.Z., and T.Z.; Investigation, L.Z., T.L., Q.X., W.H., and J.X.; Writing and Editing, J.X., L.Z., W.H.; Funding Acquisition, W.H. and J.X.; Resources, D.D., R.Z., G.H., W.H., and J.X.

Data sharing statement

Datasets for this study have been deposited into the GEO database (http://www.ncbi.nlm.nih.gov/geo/) under accession identification numbers GSE152241, GSE151927 and GSE183158.

Declaration of interests

All authors declare no competing interests.

Acknowledgements

This work was supported by the National Natural Science Foundation of China (No. 81970553, No. 82022049, J.X.; No. 82073105, N.N.; No. 81973632, W.H.); Shanghai Youth Talent Support Programme to J.X.; Shanghai Municipal Education Commission-Gaofeng Clinical Medicine Grant Support (No. 20161312, J.X.).

Supplementary materials

Supplementary material associated with this article can be found in the online version at doi:10.1016/j.ebiom.2022.103959.

References

1 Lee PJ, Papachristou GI. New insights into acute pancreatitis. *Nat Rev Gastroenterol Hepatol*. 2019;16(8):479–496.
2 Schepers NJ, Bakker OJ, Besselink MG, et al. Impact of characteristics of organ failure and infected necrosis on mortality in necrotising pancreatitis. *Gut*. 2019;68(6):1044–1051.
3 Sternby H, Bolado F, Canaval-Zuleta HJ, et al. Determinants of severity in acute pancreatitis: a nation-wide multicenter prospective cohort study. *Ann Surg*. 2019;270(2):348–355.
4 Shi N, Liu T, de la Iglesia-Garcia D, et al. Duration of organ failure impacts mortality in acute pancreatitis. *Gut*. 2020;69(3):604–605.
5 Gukovskaya AS, Gukovsky I, Algul H, et al. Autophagy, inflammation, and immune dysfunction in the pathogenesis of pancreatitis. *Gastroenterology*. 2017;153(5):1212–1226.
6 Zheng L, Xue J, Jaffee EM, Habtezion A. Role of immune cells and immune-based therapies in pancreatitis and pancreatic ductal adenocarcinoma. *Gastroenterology*. 2013;144(6):1230–1240.
7 Xue J, Habtezion A. Carbon monoxide-based therapy ameliorates acute pancreatitis via TLR4 inhibition. *J Clin Investig*. 2014;124(1):437–447.
8 Lackey DE, Olefsky JM. Regulation of metabolism by the innate immune system. *Nat Rev Endocrinol*. 2016;12(1):15–28.
9 Kubes P, Jenne C. Immune Responses in the Liver. *Annu Rev Immunol*. 2018;36:247–277.
10 Wang X, Zhao X, Shi C, et al. Potential mechanisms and significance of acute pancreatitis-associated liver injury. *Scand J Gastroenterol*. 2006;41(5):604–613.
11 Peng Y, Hong J, Raftery D, et al. Metabolomic-based clinical studies and murine models for acute pancreatitis disease: a review. *Biochim Biophys Acta Mol Basis Dis*. 2021;1867:(7) 166123.
12 Navina S, Acharya C, DeLany JP, et al. Lipotoxicity causes multisystem organ failure and exacerbates acute pancreatitis in obesity. *Sci Transl Med*. 2011;3(107):107ra10.
13 de Oliveira C, Khatua B, Noel P, et al. Pancreatic triglyceride lipase mediates lipotoxic systemic inflammation. *J Clin Investig*. 2020;130(4):1931–1947.
14 Noel P, Patel K, Durgampudi C, et al. Peripancreatic fat necrosis worsens acute pancreatitis independent of pancreatic necrosis via unsaturated fatty acids increased in human pancreatic necrosis collections. *Gut*. 2016;65(1):100–111.
15 Khatua B, El-Kurdi B, Patel K. Adipose saturation reduces lipotoxic systemic inflammation and explains the obesity paradox. *Sci Adv*. 2021;7(5):eabd6449.
16 Puchalska P, Crawford PA. Multi-dimensional roles of ketone bodies in fuel metabolism, signaling, and therapeutics. *Cell Metab*. 2017;25(2):262–284.
17 Rinaldo P, Matern D, Bennett MJ. Fatty acid oxidation disorders. *Annu Rev Physiol*. 2002;64:477–502.
18 Sabari BR, Zhang D, Allis CD, et al. Metabolic regulation of gene expression through histone acylations. *Nat Rev Mol Cell Biol*. 2017;18(2):90–101.

19 Zhang H, Tang K, Ma J, et al. Ketogenesis-generated beta-hydroxybutyrate is an epigenetic regulator of CD8(+) T-cell memory development. *Nat Cell Biol*. 2019;22(1):18–25.
20 Rahman M, Muhammad S, Khan MA, et al. The β-hydroxybutyrate receptor HCA2 activates a neuroprotective subset of macrophages. *Nat Commun*. 2014;5:3944.
21 Chen Y, Ouyang X, Hoque R, et al. β-Hydroxybutyrate protects from alcohol-induced liver injury via a Hcar2-cAMP dependent pathway. *J Hepatol*. 2018;69(3):687–696.
22 Kimura I, Inoue D, Maeda T, et al. Short-chain fatty acids and ketones directly regulate sympathetic nervous system via G protein-coupled receptor 41 (GPR41). In: *Proceedings of the National Academy of Sciences of the United States of America*. 108, 20118030–8035.
23 Youm YH, Nguyen KY, Grant RW, et al. The ketone metabolite β-hydroxybutyrate blocks NLRP3 inflammasome-mediated inflammatory disease. *Nat Med*. 2015;21(3):263–269.
24 Shimazu T, Hirschey MD, Newman J, et al. Suppression of oxidative stress by beta-hydroxybutyrate, an endogenous histone deacetylase inhibitor. *Science*. 2013;339(6116):211–214.
25 Banks PA, Bollen TL, Dervenis C, et al. Classification of acute pancreatitis-2012: revision of the Atlanta classification and definitions by international consensus. *Gut*. 2013;62(1):102–111.
26 Zhang R, Shi J, Zhang R, et al. Expanded CD14(hi)CD16(-) immunosuppressive monocytes predict disease severity in patients with acute pancreatitis. *J Immunol*. 2019;202(9):2578–2584.
27 Shi N, Liu T, de la Iglesia-Garcia D, et al. Duration of organ failure impacts mortality in acute pancreatitis. *Gut*. 2020;69(3):604–605.
28 Zandi-Nejad K, Takakura A, Jurewicz M, et al. The role of HCA2 (GPR109A) in regulating macrophage function. *FASEB J*. 2013;27 (11):4366–4374.
29 Huang W, Cane MC, Mukherjee R, et al. Caffeine protects against experimental acute pancreatitis by inhibition of inositol 1,4,5-trisphosphate receptor-mediated Ca^{2+} release. *Gut*. 2017;66(2):301–313.
30 Ou X, Cheng Z, Liu T, et al. Circulating histone levels reflect disease severity in animal models of acute pancreatitis. *Pancreas*. 2015;44(7):1089–1095.
31 Yang X, Yao L, Fu X, et al. Experimental acute pancreatitis models: history, current status, and role in translational research. *Front Physiol*. 2020;11: 614591.
32 Wu J, Zhang L, Shi J, et al. Macrophage phenotypic switch orchestrates the inflammation and repair/regeneration following acute pancreatitis injury. *eBioMedicine*. 2020;58:102920.
33 Xue J, Sharma V, Hsieh MH, et al. Alternatively activated macrophages promote pancreatic fibrosis in chronic pancreatitis. *Nat Commun*. 2015;6:7158.
34 Jung KH, Song SU, Yi T, et al. Human bone marrow-derived clonal mesenchymal stem cells inhibit inflammation and reduce acute pancreatitis in rats. *Gastroenterology*. 2011;140(3):998–1008.
35 Roch AM, Maatman TK, Cook TG, et al. Therapeutic use of adipose-derived stromal cells in a murine model of acute pancreatitis. *J Gastrointest Surg Off J Soc Surg Alimentary Tract*. 2020;24(1):67–75.
36 Knottnerus SJG, Bleeker JC, Wüst RCI, et al. Disorders of mitochondrial long-chain fatty acid oxidation and the carnitine shuttle. *Rev Endocr Metab Disord*. 2018;19(1):93–106.
37 Schoenen J. β-Hydroxybutyrate: a signaling metabolite. *Annu Rev Nutr*. 2017;37:51–76.
38 Softic S, Meyer JG, Wang GX, et al. Dietary sugars alter hepatic fatty acid oxidation via transcriptional and post-translational modifications of mitochondrial proteins. *Cell Metab*. 2019;30(4):735–753.e4.
39 Shimazu T, Hirschey MD, Hua L, et al. SIRT3 deacetylates mitochondrial 3-hydroxy-3-methylglutaryl CoA synthase 2 and regulates ketone body production. *Cell Metab*. 2010;12(6):654–661.
40 Hirschey MD, Shimazu T, Goetzman E, et al. SIRT3 regulates mitochondrial fatty-acid oxidation by reversible enzyme deacetylation. *Nature*. 2010;464(7285):121–125.
41 Bharathi SS, Zhang Y, Mohsen AW, et al. Sirtuin 3 (SIRT3) protein regulates long-chain acyl-CoA dehydrogenase by deacetylating conserved lysines near the active site. *J Biol Chem*. 2013;288(47):33837–33847.
42 Longo N, Frigeni M, Pasquali M. Carnitine transport and fatty acid oxidation. *Biochim Biophys Acta*. 2016;1863(10):2422–2435.
43 Habtezion A, Gukovskaya AS, Pandol SJ. Acute pancreatitis: a multifaceted set of organelle and cellular interactions. *Gastroenterology*. 2019;156(7):1941–1950.
44 Chen X, Barozzi I, Termanini A, et al. Requirement for the histone deacetylase Hdac3 for the inflammatory gene expression program in macrophages. In: *Proceedings of the National Academy of Sciences of the United States of America*. 109, 2012E2865–E2874.
45 Glozak MA, Sengupta N, Zhang X, et al. Acetylation and deacetylation of non-histone proteins. *Gene*. 2005;363:15–23.
46 Kiernan R, Bres V, Ng RW, et al. Post-activation turn-off of NF-kappa B-dependent transcription is regulated by acetylation of p65. *J Biol Chem*. 2003;278(4):2758–2766.
47 Rakonczay Z, Hegyi P, Takacs T, et al. The role of NF-kappaB activation in the pathogenesis of acute pancreatitis. *Gut*. 2008;57 (2):259–267.
48 Zhang T, Xia M, Zhan Q, et al. Sodium butyrate reduces organ injuries in mice with severe acute pancreatitis through inhibiting HMGB1 expression. *Dig Dis Sci*. 2015;60(7):1991–1999.
49 Bombardo M, Saponara E, Malagola E, et al. Class I histone deacetylase inhibition improves pancreatitis outcome by limiting leukocyte recruitment and acinar-to-ductal metaplasia. *Br J Pharmacol*. 2017;174(21):3865–3880.
50 Stubbs BJ, Newman JC. Ketogenic diet and adipose tissue inflammation-a simple story? Fat chance!. *Nat Metab*. 2020;2(1):3–4.
51 Watanabe M, Tozzi R, Risi R, et al. Beneficial effects of the ketogenic diet on nonalcoholic fatty liver disease: a comprehensive review of the literature. *Obes Rev Off J Int Assoc Study Obes*. 2020;21 (8):e13024.
52 Lu Y, Yang YY, Zhou MW, et al. Ketogenic diet attenuates oxidative stress and inflammation after spinal cord injury by activating Nrf2 and suppressing the NF-κB signaling pathways. *Neurosci Lett*. 2018;683:13–18.
53 Harun-Or-Rashid M, Inman DM. Reduced AMPK activation and increased HCAR activation drive anti-inflammatory response and neuroprotection in glaucoma. *J Neuroinflamm*. 2018;15(1):313.
54 Garg PK, Singh VP. Organ failure due to systemic injury in acute pancreatitis. *Gastroenterology*. 2019;156(7):2008–2023.
55 Biczo G, Vegh ET, Shalbueva N, et al. Mitochondrial dysfunction, through impaired autophagy, leads to endoplasmic reticulum stress, deregulated lipid metabolism, and pancreatitis in animal models. *Gastroenterology*. 2018;154(3):689–703.
56 Mukherjee R, Mareninova OA, Odinokova IV, et al. Mechanism of mitochondrial permeability transition pore induction and damage in the pancreas: inhibition prevents acute pancreatitis by protecting production of ATP. *Gut*. 2016;65(8):1333–1346.
57 Shalbueva N, Mareninova OA, Gerloff A, et al. Effects of oxidative alcohol metabolism on the mitochondrial permeability transition pore and necrosis in a mouse model of alcoholic pancreatitis. *Gastroenterology*. 2013;144(2):437–446. e6.
58 Cherry AD, Piantadosi CA. Regulation of mitochondrial biogenesis and its intersection with inflammatory responses. *Antioxid Redox Signal*. 2015;22(12):965–976.
59 Blüher M. Obesity: global epidemiology and pathogenesis. *Nat Rev Endocrinol*. 2019;15(5):288–298.
60 Wu D, Zhang M, Xu S, et al. Nonalcoholic fatty liver disease aggravated the severity of acute pancreatitis in patients. *Biomed Res Int*. 2019;2019: 9583790.
61 Hou S, Tang X, Cui H, et al. Fatty liver disease is associated with the severity of acute pancreatitis: a systematic review and meta-analysis. *Int J Surg*. 2019;65:147–153.
62 Vancsa S, Nemeth D, Hegyi P, et al. Fatty liver disease and non-alcoholic fatty liver disease worsen the outcome in acute pancreatitis: a systematic review and meta-analysis. *J Clin Med*. 2020;9 (9):2698.
63 Zhang R, Deng L, Jin T, et al. Hypertriglyceridaemia-associated acute pancreatitis: diagnosis and impact on severity. *HPB: Off J Int Hepato Pancreato Biliary Assoc*. 2019;21(9):1240–1249.
64 Umpierrez G, Korytkowski M. Diabetic emergencies-ketoacidosis, hyperglycaemic hyperosmolar state and hypoglycaemia. *Nat Rev Endocrinol*. 2016;12(4):222–232.
65 Vege SS, DiMagno MJ, Forsmark CE, et al. Initial medical treatment of acute pancreatitis: American gastroenterological association institute technical review. *Gastroenterology*. 2018;154(4):1103–1139.
66 Moggia E, Koti R, Belgaumkar AP, et al. Pharmacological interventions for acute pancreatitis. *Cochrane Database Syst Rev*. 2017;4: CD011384.
67 Yang X, Zhang R, Jin T, et al. Stress hyperglycemia is independently associated with persistent organ failure in acute pancreatitis. *Dig Dis Sci*. 2021. https://doi.org/10.1007/s10620-021-06982-8.